Chemical Science

EDGE ARTICLE

View Article Online
View Journal | View Issue

Cite this: *Chem. Sci.*, 2019, **10**, 8817

All publication charges for this article have been paid for by the Royal Society of Chemistry

Received 8th February 2019
Accepted 2nd August 2019

DOI: 10.1039/c9sc00690g

rsc.li/chemical-science

Mechanistic studies of a "Declick" reaction†

Margaret K. Meadows,‡[a] Xiaolong Sun,‡[b] Igor V. Kolesnichenko,[c] Caroline M. Hinson,[d] Kenneth A. Johnson*[e] and Eric V. Anslyn*[d]

A kinetic analysis of a "declick" reaction is described. Compound **1**, previously reported to couple an amine and a thiol (*i.e.* "click") under mild aqueous conditions to create **2**, undergoes release of the unaltered coupling partners upon triggering with dithiothreitol (**DTT**). In the study reported herein various aniline derivatives possessing para-electron donating and withdrawing groups were used as the amines. UV/vis spectroscopy of the declick reaction shows time-dependent spectra lacking isosbestic points, implying a multi-step mechanism. Global data fitting using numerical integration of rate equations and singular value decomposition afforded the spectra and time-dependence of each species, as well as rate constants for each step. The kinetic analysis reveals a multi-step process with an intermediate where both thiols of **DTT** have added prior to expulsion of the aniline leaving group, followed by rearrangement to the final product. Hammett plots show a negative rho value on two of the steps, indicating positive charge building (*i.e.* reduction of a negative charge) in the step leading to the intermediate and its rate-determining breakdown. Overall, the kinetic study reported herein gives a complete mechanistic picture of the declick reaction.

Introduction

Recently our group reported compound **1**, a simple derivative of Meldrum's acid, which is capable of coupling (*i.e.* clicking) amines and thiols (Scheme 1).[1] Using **1**, mono-addition of a primary amine followed by exchange of the thiol occurs in a 5 : 1 pH 7 phosphate buffer : acetonitrile mixture with sparging to give structures such as **2**. The amine and thiol can be recovered upon addition of cysteine or dithiothreitol (**DTT**), what we referred to as a "declick". This returns the original amine and thiol without modification and generates product **3**.

Interestingly, structure **2** does not declick with β-mercaptoethanol (**BME**), which is essentially half the structure of **DTT**. Instead, the thiols exchange to give **4**, with no removal of the amine.[2] This observation suggests that the second thiol of **DTT** plays an essential role in the declicking mechanism of **2**. This is in contrast to the reaction of **1** with **BME**, which we previously have shown is a second order reaction, first order in both **1** and **BME**, in which the UV/vis spectra have two observable species (reactant **1** and product **5**) with isosbestic points.[2] Thus, while **BME** can remove two thiols from **1**, **DTT** is required to remove an amine and a thiol from **2**.

To explain the difference between the reactivity of **2** with **DTT** and **BME**, we previously postulated the intermediacy of a seven-membered ring (*i.e.* **6**) that rearranges to **3**.[1,2] Hence, to study this reaction in detail and confirm or refute such an intermediate, we commenced a mechanistic analysis of the declicking

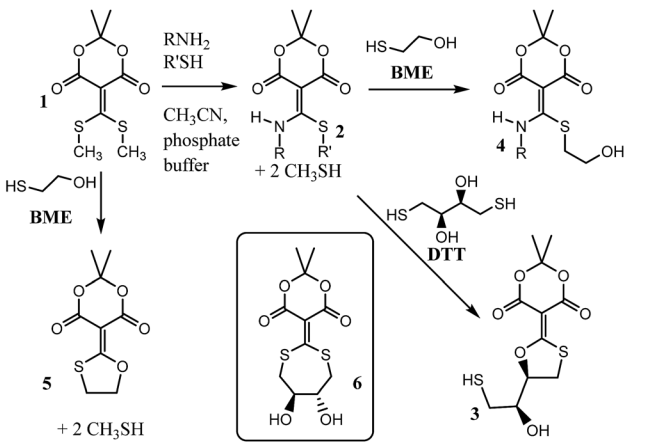

Scheme 1 General scheme for the coupling of an amine and thiol using **1**, and the "declicking" using **DTT** or **BME**.

[a]*Department of Chemistry, Mercer University, 1501 Mercer University Dr., Macon, Georgia 31207, USA*

[b]*The Key Laboratory of Biomedical Information Engineering of Ministry of Education, School of Life Science and Technology, Xi'an Jiaotong University, Xi'an 710049, P. R. China*

[c]*Photovoltaics & Materials Technology Department, Sandia National Laboratories, PO Box 5800, MS 0734, Albuquerque, New Mexico 87185, USA*

[d]*Department of Chemistry, University of Texas at Austin, Austin, Texas 78712, USA. E-mail: anslyn@austin.utexas.edu*

[e]*Institute for Cellular and Molecular Biology, Department of Molecular Biosciences, University of Texas, Austin, Texas 78712, USA*

† Electronic supplementary information (ESI) available: Characterization, spectra, kinetics, computer fits. See DOI: 10.1039/c9sc00690g

‡ These authors contributed equally.

reaction with **DTT** and several versions of **2** where the R-groups were aniline derivatives (referred to herein as **2Ph**-X, where X is a variety of substituents). The study primarily relies on kinetics, which turned out to be more complicated than expected, but which definitely supports a mechanism involving intermediate **6**, as well as other unanticipated intermediates and products as described here.

Kinetics play a key role in mechanistic physical organic methods to define the chemical steps involved in complex organic transformations.[3,4] Rigorous kinetic analysis can determine the pathway of a reaction and identify intermediates.[5,6] In performing kinetic analysis, a common approach is to derive an integrated form of the rate equations. For more complex models, simplifying approximations needed to solve the equations may not be valid and fitting data to multiple exponential functions is unreliable. Fitting data based on numerical (rather than analytical) integration of rate equations overcomes the limitations of conventional fitting and returns intrinsic rate constants rather than eigenvalues.[7] In addition, fitting time-dependent spectra based on singular value decomposition allows complex observable spectra to be deconvoluted to reveal the underlying spectra and time-dependence of each species.[8–10]

Here we combine the use of singular value decomposition (SVD) with numerical integration of rate equations to globally fit time-resolved spectra collected at several concentrations of reactants. The approach provides intrinsic rate constants for each step in the reaction and defines the spectra for each species. Confidence contour analysis provides a robust assessment of the extent to which each rate constant is constrained by the data.[11–13]

Results and discussion

In our efforts to better understand the declicking mechanism, we employed aniline derivatives of **2** instead of the previously reported primary alkyl amines. This imparted a chromophore to the structures and allowed us to vary the electronics *via* substituent changes (–X) on the *para* position (**2Ph**-X). Aniline adds cleanly to conjugate acceptor **1** in pH 7 phosphate buffer/acetonitrile (5 : 1) to give **2** (R═Ph, R′═CH_3) in the same fashion as previously reported for primary alkyl amines.[1] A range of *p*-substituted anilines with both electron donating and electron withdrawing groups were tested and each were found to be capable of displacing methyl mercaptan from **1** (Table 1). Full characterization of each derivative **2Ph**-X is given in the ESI Section VII.†

Prior to examining the kinetics of the reactions of **2Ph**-X's with **DTT**, we sought to determine any pH dependence that may be involved. Hence, the pK_a of each derivative of **2Ph**-X (eqn (1), and Table 1) was determined *via* standard potentiometric titration in a (2 : 1) H_2O/MeOH mixture (ESI Fig. S1 to S6†). The values range between 4.34 and 6.65, with the expected trend of more electron withdrawing groups showing a lower pK_a and electron donating groups increasing the pK_a. The relationship between these pK_a values was described *via* a Hammett linear free energy relationship (LFER) (Fig. 1).[14] This Hammett plot

Table 1 Derivatives of **2** used in this study: X-group, compound number, and pK_a. In all cases, R′ (as delineated in Scheme 1) is CH_3

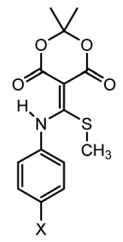

2PH-X

X	#	pK_a
H	**2Ph**-H	6.02
CH_3	**2Ph**-CH_3	6.51
OCH_3	**2Ph**-OCH_3	6.54
Br	**2Ph**-Br	5.56
CN	**2Ph**-CN	4.54
NO_2	**2Ph**-NO_2	4.34

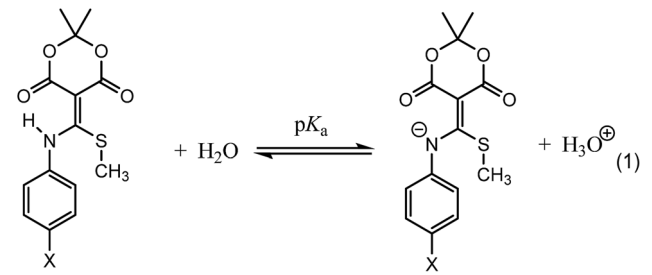

2PH-X **2PH**-X^- (1)

reveals a rho value of 2.4, indicating that the sensitivity of this acid/base reaction is greater than that of the ionization of benzoic acid.

As a second control study, prior to the analysis of the kinetics of the aniline derivatives of **2Ph**-X with **DTT**, we confirmed that **2Ph**-H would not "declick" the aniline upon reaction with **BME**,

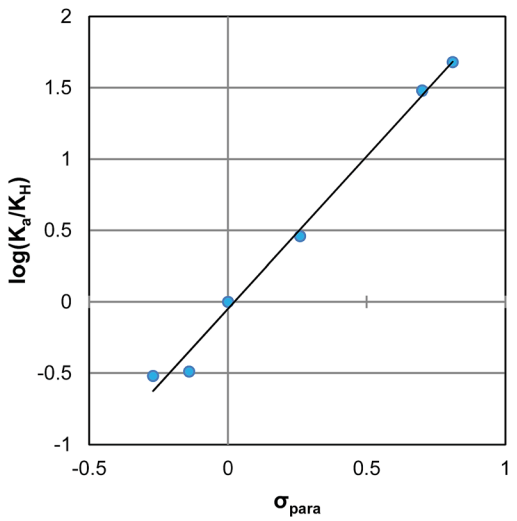

Fig. 1 Hammett plot for the ionization of compounds **2Ph**-X (Table 1).

as we previously found would not occur with alkyl amine versions of **2**. Indeed, upon stirring **2Ph**-H with **BME** there were only slight UV/vis spectral changes (Fig. S7†), while LCMS detected incorporation of **BME** in place of methyl mercaptan. Thus, while thiols dynamically scramble with the **2Ph**-X compounds, **BME** does not lead to release of the aniline.

Kinetic analysis of 2Ph-H in detail

Fig. 2 shows the time-dependent UV/vis traces of the reaction of **2Ph**-H with **DTT** in pH 6.8 (2 : 1) H_2O/MeOH mixture. As can be observed, there is a lack of isosbestic points, meaning that one or more intermediates are spectroscopically observable, and the reactions proceed at rates such that the individual steps are not separated cleanly with time during the reaction. Moreover, this means that reactions can be detected that precede the rate-determining step (rds) of the reaction. The time dependent traces of the other **2Ph**-X groups are given in the ESI† and are analogous. In an unpublished study using alkylamine versions of **2** rather than anilines, the kinetics is much simpler and shows isosbestic points. To analyze a complex scenario without isosbestic points, we turned to SVD methods,[8–10,15,16] that afforded the spectra of each kinetically-significant species and rate constants for each step of the reaction.

In fitting the data based on SVD, we included independent UV/vis spectra of known species to reduce the number of variables. In particular, we included the spectra of the anilines (**An**-X), **DTT**, and the postulated final product **3** (Scheme 1). The spectrum of the reactant is well defined by the data at time = 0, so it was not included as a known entity.

We thus only needed to independently generate **3**, which was done through a preparative reaction between **1** and **DTT** in acetonitrile, followed by isolation and full characterization (see ESI Section III†). The UV/vis spectra of **3** showed a λ_{max} at 290 nm, which was consistent with similar other geminal S- and O-vinylethers of Meldrum's acid we have previously reported.[1,2] However, upon monitoring the spectra of **3** at 50 μM in the solvent system in which the reaction of **2Ph**-H and **DTT** was performed in H_2O/MeOH (2 : 1) pH 6.8, it was observed that spectral changes occurred (Fig. 3), with the λ_{max} shifting from

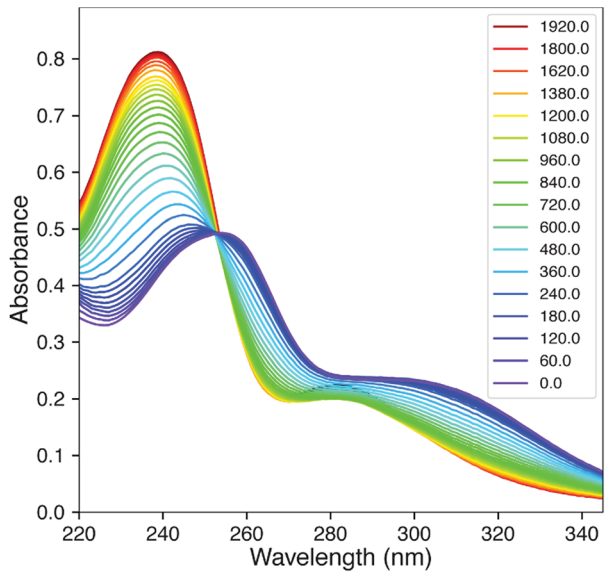

Fig. 2 UV/vis traces for the reaction between **2Ph**-H with **DTT** over time (minutes, insert values). Fit of time resolved spectra collected at 5 mM **DTT**; lines represent data and dots are the reconstituted spectra.

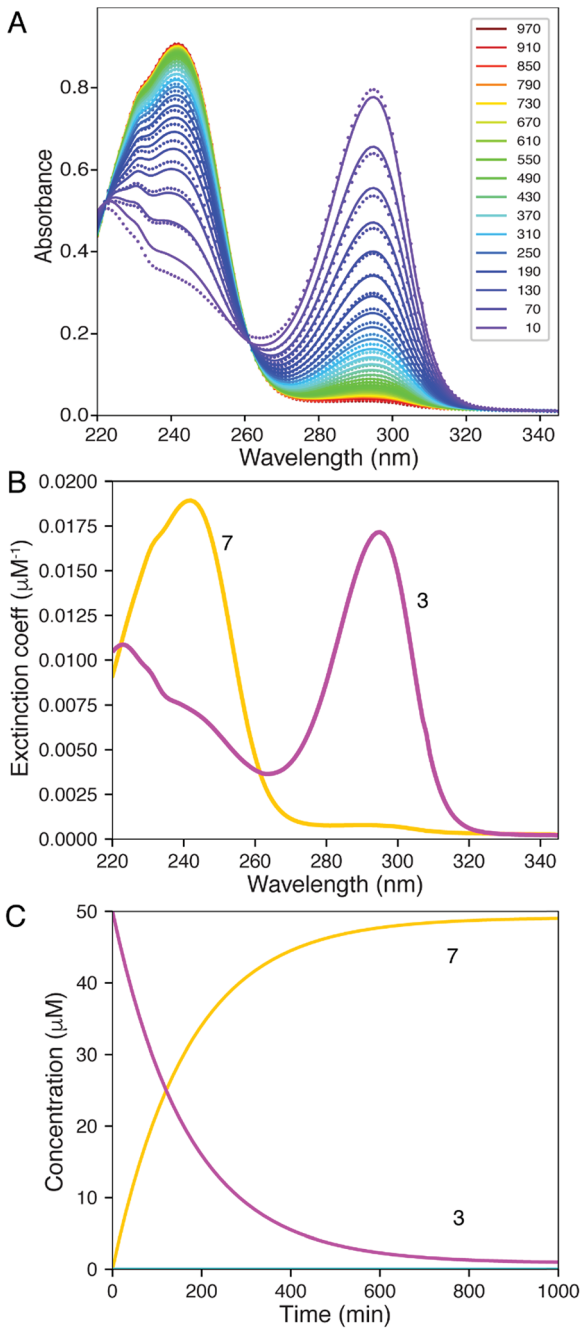

Fig. 3 (A) Time course for the UV-vis absorbance spectra of the reaction of **3** (50 μM) to form **7** after being placed in a 2 : 1 H_2O : MeOH mixture at pH 6.8. The dots show the experimental data, while the solid lines show the fitted curve. The peak at 240 nm increases while the peak at 295 nm decreases. (B) Spectra derived from fitting **3**, magenta; **7**, yellow. (C) Time dependence of conversion of **3** (magenta) to **7** (yellow).

295 nm to 240 nm over a period of approximately 20 minutes (Fig. 3A, and ESI Fig. S9†).

The shifting to a lower wavelength is indicative of a lowering of the conjugation where the resulting spectrum was reminiscent of the spectrum of the conjugate base of Meldrum's acid. Thus, we postulated the generation of compound **7** (eqn (2), color coded to match Fig. 3). As a control, we analysed the UV/vis spectra of compound **5** (Scheme 1) under the same conditions, and there was no change with time (ESI Fig. S10†), confirming that the second thiol is involved in the creation of **7**. The rate constant for conversion of **3** to **7** is well-defined, 0.006 min^{-1}, but the rate of reaction of **7** to **3** is less well-defined, ~0.0001 min^{-1}, giving an equilibrium constant of 60 favouring **7**.

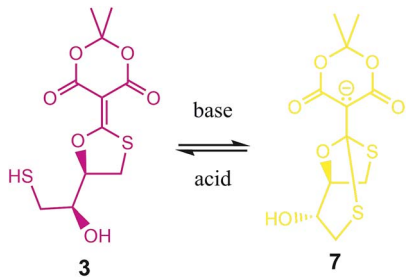

(2)

To verify that **7** was the species created, we postulated that the equilibrium between **3** and **7** should be pH dependent. Compound **7** was expected to dominate at higher pHs while **3** should dominate at lower pHs (eqn (2)). The pH dependence of this equilibrium should pivot around the pK_a of Meldrums acid, *i.e.* near pHs 5–6. To confirm our hypothesis, we carried out the addition of sodium hydroxide and hydrogen chloride aqueous solutions (Fig. 4). We could switch between a dominance of the λ_{max} at 240 nm (**7**) to 290 nm (**3**) depending upon the addition of base or acid, respectively. Importantly, we note that in our previous studies of the reactions of **1** or **2** with **DTT** we failed to recognize the formation of **7** because the product was always isolated from organic media, where it reverts to structure **3**.

With the knowledge that the actual product was compound **7** wherein two thiols have undergone conjugate addition generating an anionic bicyclic system, we realized that other intermediates analogous to **7** could be present in the mechanism. Thus, a step-by-step picture (minus proton transfers) was generated in advance of kinetic modelling taking this possibility into account (Scheme 2). Further, with this scheme in mind, it seemed evident that the rds of such a process could be the loss of aniline (k_2), or potentially the cyclization to **7** (k_3). Thus, we expected to observe some of these compounds in the ^{1}H-NMR spectra as they build up prior to the rds. In fact, potentially three structures in addition to the reactant **2Ph**-X and products **3**/**7** would be observable: **8Ph**-X, **9Ph**-X, and intermediate **6**. In actuality, that proved to be the case. When using **2Ph**-NO_2 (the slowest of the reactants), the ^{1}H-NMR spectra revealed two unknown species, one of which contained aniline, but was not *p*-nitroaniline, nor the reactants/products (Fig. S10†). Both species build up with time and then decreased as the reaction approached completion. Based upon a kinetic analysis that is best fit with a rapid conversion of **8Ph**-X to **9Ph**-X (see below), we postulate these species to be **9Ph**-X and **6**.

To analyse the kinetics of the reactions of **2Ph**-X's with **DTT**, we devised a series of mechanistic postulates. Several were tested, but the one that fit the data well is embodied in Scheme 2. In this mechanism, an initial second order reaction with **DTT** leads to a thiol conjugate addition, undoubtedly in a reversible fashion with **CH_3SH** readdition, but upon loss of methyl mercaptan the reaction is driven in an irreversible direction due to a subsequent rapid first-order intramolecular thiol addition. Thus, we modelled the first conjugate addition and loss of **CH_3SH** together in a single step, as well as the fast cyclization step, as sequential irreversible reactions. The resulting **9Ph**-X was postulated to have a long enough lifetime to build up and be spectroscopically observable prior to the step that generates the aniline chromophore, as does **6** before converting to an equilibrium of **3** and **7**, and hence the lack of isosbestic points in Fig. 2. After loss of aniline to generate **6**, slow intramolecular cyclization occurs to set up the equilibrium between **3** and **7**.

Thus, having obtained UV/vis spectra of aniline, as well as products **3** and **7**, we set out to fit the spectral data of Fig. 2 in detail using **2Ph**-H and including the data in Fig. 3A. In addition, assignment of chemical structures to various intermediates was made by comparisons to analogous isolable structures, as now described.

Here we have used SVD to deconvolute the spectra and time-dependence of species from analysis of time-resolved spectra using KinTek Explorer kinetic modelling software.[17] The output of the SVD analysis is a set of vectors defining the amplitude *versus* time and spectra (absorbance *versus* wavelength). The product of the amplitude and spectra vectors reconstitutes the matrix to account for the observed data; SVD provides a mathematically sound solution, but one that lacks physical reality.[10] We then fit the amplitude vectors based upon the chosen model to derive realistic time dependence of the reaction and spectra of each species.[18]

Our analysis first focused upon the complete declicking mechanism of **2Ph**-X with X = H (*i.e.* **2Ph**-H) (50 μM) with **DTT** at concentrations of 1, 2, 5 and 10 mM. The mechanism was separated into steps analogous to those postulated in Scheme 2, which results in the possibility of several calculated rate constants to be modelled, for example k_1, k_2, k_3, k_4 and k_{-4} (species, spectra, time-courses are color-coded in Fig. 4 to correspond to the colours in Scheme 2). The addition of **DTT** is a second-order reaction (k_1), followed by a cyclization to generate **9Ph**-H. Upon attempting to model the kinetics including this cyclization step, a good fit with low residuals (such as that described below) could never be achieved, and the resulting calculated absorbance spectra did not make sense for the expected chromophore that **9Ph**-H would show. Thus, we left this step out, meaning that the cyclization is rapid (referred to as fast in Scheme 2). In addition, k_4 and k_{-4} represent the equilibrium between **3** and **7** which was modelled from the data of Fig. 3. These steps were also not necessary for the global fit,

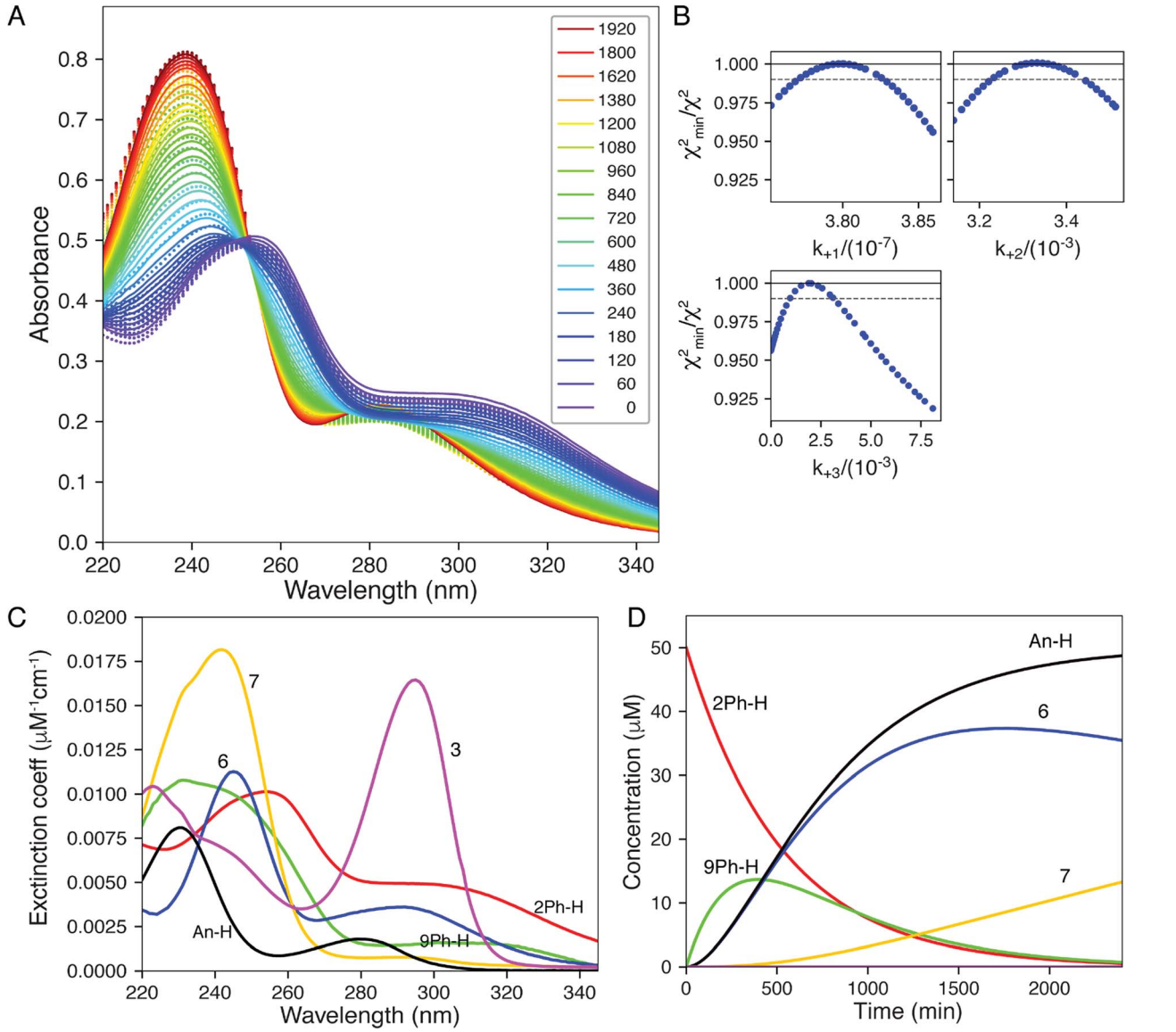

Fig. 4 Global fitting of time-resolved spectra. Spectra were collected as a function of time after mixing 1, 2, 5, and 10 mM **DTT** with **2Ph**-H (50 uM) and were fit globally. (A) Time-resolve spectra collected at 5 mM **DTT**. The dots show the data and the lines give the fitted curve. The inset shows the color-coded time for collection of each spectrum (min). (B) Confidence contour analysis; the dashed line shows the χ^2 threshold (0.98) used to establish confidence intervals. (C) Spectra of individual species resolved by global data fitting. (D) Time dependence of individual species predicted by the global fitting. All data were fit globally to derive the rate constants listed in Table 2. Colours correspond to Scheme 2: **2Ph**-H (red), **9Ph**-H (green), **6** (blue), **An**-H (black), **7** (yellow) and **3** (magenta).

likely because this equilibration is past the rds of the mechanism and the equilibrium favours **7**.

While the first step of Scheme 2 is undoubtedly an equilibrium, the loss of methyl mercaptan (a gas) from **2Ph**-H and the rapid cyclization pushes the equilibria to **8Ph**-H. In addition, as discussed in the previous paragraph, intramolecular conjugate addition of the dangling thiol to generate **9Ph**-H is postulated to be fast, which is anticipated by the high nucleophilicity and effective molarity of the thiol, pushing this equilibrium to **9Ph**-H. Thus, the step from **2Ph**-H to **9Ph**-H was modelled as a single step. Loss of aniline (**An**-H) was anticipated to be rate determining (k_2). The time-course data reveals that the k_1 and k_2 steps do not occur as completely distinct steps as a function of time (Fig. 2) because isosbestic points are not observed in the spectra (*i.e.*, no clean 1-to-1 stoichiometric interconversions without accompanying further reactions during the time course of the reaction). After loss of aniline, cyclization occurs to generate **7** (k_3) which very slowly forms **3**. This equilibrium between **3** and **7** was derived independently, as discussed above. However, although this equilibration is slow on the timescale of data collection, it was still included in fitting the time-resolved spectral data. The data on the conversion of **3** to **7** were included in the global data fitting because they provide their spectra.

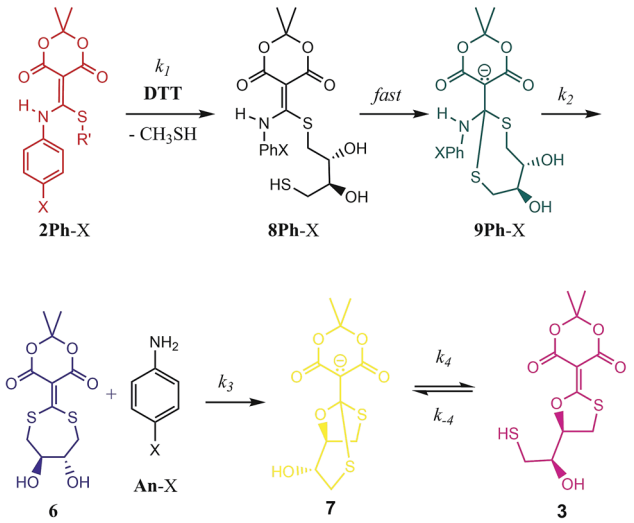

Scheme 2 Mechanistic scenario that could be used to properly fit the UV/vis traces (Fig. 2) for the reaction of **2Ph**-X and **DTT**. The structures are color-coded to correspond with their spectra and time course data in Fig. 4 (as well as ESI Fig. S12–S15†).

The global data fitting revealed that a step past the departure of aniline was required to generate a model with low residuals and spectra that made sense for the various structures depicted in Scheme 2. Yet, this rate constant was not well defined. The best fit settled upon a k_3 of 2.00×10^{-4} min^{-1}, but with large errors. Although k_3 was not well-defined, this step was required to achieve a good fit, as evaluated by minimal χ^2 and reasonable output spectra. In fitting the data collected using various derivatives, the value of $k_3 = 2.00 \times 10^{-4}$ min^{-1} was chosen as a maximum value sufficient to give an optimal fit for all experiments. We chose a maximum value, such that greater values improperly fit the data. Lower values had only small effects on χ^2, but gave unrealistic spectra. Accordingly, we used the value of $k_3 = 2.00 \times 10^{-4}$ min^{-1} for all the **2Ph**-X species, because this step is common to all the derivatives. The value is smaller than, but similar to, the k_2 rate constant (see Table 2) that involves the loss of aniline. Hence, the intermediate **6** is expected to build up, as will be discussed below. The fact that k_2 and k_3 were very close is part of why k_3 was so difficult to define accurately. In summary, the entire kinetic profile of **2Ph**-H was nicely fit with k_1 and k_2 values shown in Table 2.

Table 2 Summary of rate constants for **2Ph**-X's (ESI Fig. S12–S15). Rate constants were derived by global fitting of the time-resolved spectra collected at 1, 2, 5 and 10 mM **DTT**. Standard error estimates were derived from confidence contour analysis with a χ^2 threshold of 0.95 (see Fig. 4B). Values in brackets were locked in fitting, and are not necessarily correct. Data for derivatives other than **2Ph**-H were fit to a simple 3-step model and k_3 was locked at a maximum value sufficient to give a good fit

	$k_1 \times 10^{-1}$ (M^{-1} min^{-1})	$k_2 \times 10^{-3}$ (min^{-1})	$k_3 \times 10^{-4}$ (min^{-1})
2Ph-H	3.8 ± 0.03	3.26 ± 0.01	2.00 ± 1.4
2Ph-OMe	4.31 ± 0.02	3.14 ± 0.01	[2.00]
2Ph-OH	4.52 ± 0.06	4.5 ± 0.1	[2.00]
2Ph-Br	2.77 ± 0.03	1.98 ± 0.06	[2.00]
2Ph-NO_2	1.94 ± 0.02	1.68 ± 0.02	[2.00]

The computer derived spectra in Fig. 4A make good chemical sense. For example, the spectra of **9Ph**-H (green) and **7** (yellow) are very similar, both analogous to the conjugate base of Meldrum's acid. Further, the spectrum of **3** (magenta) nicely matches the anticipated spectra from Fig. 3. Importantly, the spectrum of **6** (blue) has the greatest difference from the other spectra. While the two maxima of **6** are of similar wavelength to the other species, the absorbance is most like that of compound **1**.

The time course of the spectra given in Fig. 4C are also informative. Intermediate **9Ph**-H builds up in the beginning (green trace) while intermediate **6** (blue) simultaneously builds with the same rate as the creation of **An**-H (cyan), just as predicted by the mechanism. Yet, the final products **3** and **7** gradually evolve with a decrease of **6** toward the end of the reaction and are not completely formed even after 2000 minutes (yellow trace). This shows that the rate-determining step for the overall transformation is some combination of k_2 and k_3, involving the creation of **6** and its first-order rearrangement to **3** and **7**. In support, at long time scales (several hours), the ^{1}H-NMR spectra (albeit at different concentrations, see ESI†) show peaks indicative of a highly symmetrical intermediate (*i.e.* **6**) that gradually fades to the product (Fig. S10†).

After having achieved a good fit for **2Ph**-H, we turned to an analysis of the dependence of the rates upon **DTT** concentration for all **2Ph**-X species. Spectra were collected as a function of time after mixing each **2Ph**-X (50 μM) with **DTT** again at concentrations of 1, 2, 5 and 10 mM (ESI, Fig. S15–S19†). Absorbance spectra of **DTT** were subtracted from the data at each concentration. The corrected spectra were then subjected to SVD analysis using the KinTek software to derive spectra and amplitude vectors. The amplitude vectors derived at each concentration were then fit globally for all four **DTT** concentrations used to derive a single set of rate constants for each of the derivatives of **2Ph**-X (Table 2), but using the k_3 value found for **2Ph**-H. The known spectrum of each substituted aniline (**An**) was included in deriving the best global fit. The spectrum of **2Ph**-X was not included because it is well defined by the data at short time intervals. Because the slowest step of the reaction of **2Ph**-H was found to be the conversion of **6** to the mixture of products (**3** and **7**), we simplified the SVD modelling for the other **2Ph**-X derivatives to only a two-step mechanism with the set rate constant for step 3. The two rate constants for each derivative are shown in Table 2.

The rho (ρ) values of the Hammett plots are informative as to various aspects of the declick mechanism. The negative ρ (slope) values for k_1 (−0.32) and k_2 (−0.34) show that the transformations from **2Ph**-X species to **9Ph**-X species, and from **9Ph**-X species to **6** + **An**-X have an overall decrease of negative charge (Fig. 5). In order to understand these Hammett plots, a detailed analysis of the individual reactions required in the composite steps reflected by the k_1 and k_2 rate constants is required. An expanded mechanism for **DTT**-induced declicking

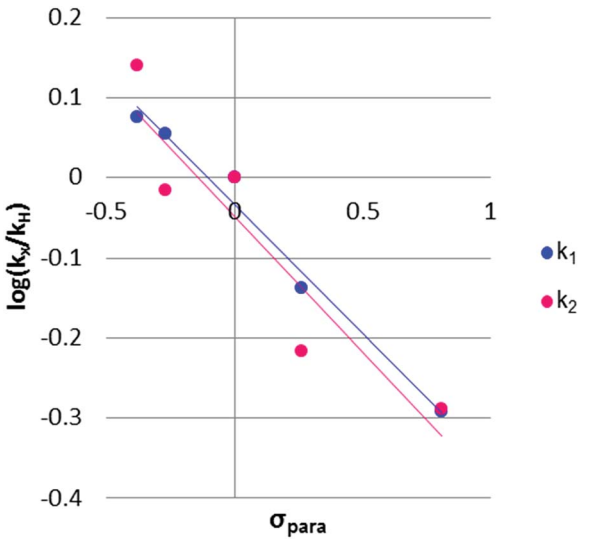

Fig. 5 Hammett plots for the two individual rate constants for the **2Ph**-X derivatives. Trendlines for k_1 ($y = -0.32x - 0.033$) and k_2 ($y = -0.34x - 0.047$) are shown.

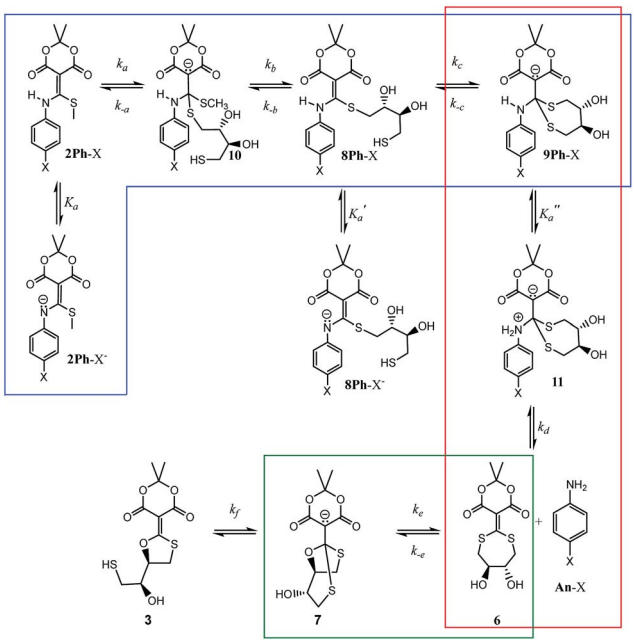

Scheme 3 A more detailed analysis of the individual steps that are embodied in the three rate constants. The blue box shows the steps in k_1, the red box those of k_2, and finally the green box those of k_3.

is shown in Scheme 3. The blue box indicates the reactions reflected by k_1, the red box indicates the reactions involved in k_2, and the green box covers the processes involved in k_3. A key to the analysis is to realize that the pH used in the kinetics is above the pK_a of each of the reactants (see Table 1, where K_a is used in the kinetic expression for eqn (3)). Thus, a significant portion of each **2Ph**-X species is ionized at the start of the reaction (**2Ph**-X$^-$). We can therefore assume that the equilibrium between **2Ph**-X$^-$ and **2Ph**-X commences the reaction with an extent of negative charge on the reactant.

In order for nucleophilic addition of **DTT** to occur, each **2Ph**-X species must be in a neutral form in order to be electrophilic. Hence, in the mechanism there is a negative charge decreasing on the nitrogen of the substituted aniline upon each **2Ph**-X$^-$ species transforming to a **9Ph**-X species. A kinetic expression for this step assuming that the expulsion of **CH_3SH** is not reversible, and using the steady-state approximation (SSA) on **8Ph**-X and **10** (Scheme 3), is given in eqn (3) (see ESI† for the derivation). Further, there is an equilibrium between **8Ph**-X and **8Ph**-X$^-$ (K_a'). However, this is a side equilibrium not involved directly in the mechanism and thus is not relevant to the kinetics. While we fully realize that the SSA for **10** and **8Ph**-X is not valid under these circumstances, the mathematical form of the rate law (eqn (3)) reveals the dependence of hydronium, *i.e.* the addition of a positive charge, thereby revealing the source of the negative rho value. For an alkyamine version of **2**, a negative rho value is therefore not expected.

$$\frac{d[\mathbf{9Ph}\text{-X}]}{dt} = \frac{k_a k_b [H_3O^+][\mathbf{2Ph}\text{-X}^-][\mathbf{DTT}]}{K_a(k_{-a} + k_b)} \quad (3)$$

The rate constant k_2 embodies the reactions from **9Ph**-X to **6** + **An**-X (red box). We postulate that a protonation of the aniline nitrogen (**11**) is required prior to its elimination. Thus, an acid equilibrium constant K_a'' is involved, along with an equivalent of hydronium. If we assume a rapidly established acid/base equilibrium with structure **11**, we derive eqn (4). The necessary protonation of the aniline leaving group explains the negative rho value. Clearly k_2 is dominated by the protonation state changes, as revealed by the negative rho-value. In fact, both k_1 and k_2 involve a protonation of the aniline, *i.e.* meaning that the rho values may be expected to be similar – but it is likely a coincidence they are so close. Albeit the protonation of the aniline may dominate the k_1 and k_2 Hammett rho values, clearly any of the other steps involved in these rate constants will also have an influence, sometimes counter to the influence of protonation on rho. Thus, this Hammett sensitivity parameter reflects several steps.

$$\frac{d[\mathbf{6}]}{dt} = \frac{k_d [H_3O^+][\mathbf{9Ph}\text{-X}]}{K_a''} \quad (4)$$

Conclusion

A kinetic analysis of the reactions of structures **2Ph**-X with **DTT** for the release of aniline and methyl mercaptan has been performed. The kinetics are complex due to a second order step prior to two first order steps of comparable rates, which together contribute to determine the net rate. This results in UV/vis time-course spectra lacking isosbestic points, thereby reflecting reactions that commence consecutively before the reaction is complete. Data were fit using numerical integration of the rate equations and based on SVD analysis, giving rate constants, spectra of intermediates, and time-course evolution

of the intermediates and products that support a proposed mechanism for the "declick" reaction. The data and fitting are consistent with negative Hammett rho values, and a complex mechanism involving intramolecular cyclizations, a 7-membered ring structure **6** as an intermediate, and an equilibrium between a bicyclic and tricyclic equilibrium of the product structures **3** and **7**. Importantly, the study highlights the power of a rigorous kinetic analysis to decipher complex chemical mechanisms.

Conflicts of interest

Financial conflict of interest statement: KAJ is President of KinTek Corporation which markets the KinTek Explorer software used in this study.

Acknowledgements

We gratefully acknowledge the support of the Welch Regents Chair (F-0046) to EVA, NSF CHE-1665037, The Center for Dynamics and Control of Materials supported by the NSF (DMR-1720595), and by The Welch Foundation grant F-1604 to KAJ.

Notes and references

1 K. L. Diehl, I. V. Kolesnichenko, S. A. Robotham, J. L. Bachman, Y. Zhong, J. S. Brodbelt and E. V. Anslyn, *Nat. Chem.*, 2016, **8**, 968.
2 X. Sun and E. V. Anslyn, *Angew. Chem., Int. Ed.*, 2017, **56**, 9522.
3 E. V. Anslyn and D. A. Dougherty, *Modern Physical Organic Chemistry*, University Science Books, 2006, pp. 355–487.
4 F. A. Carey and R. J. Sundberg, *Advanced Organic Chemistry: Part A: Structure and Mechanisms*, Springer Science & Business Media, 2007, pp. 253–388.
5 K. S. Anderson, J. A. Sikorski and K. A. Johnson, *Biochemistry*, 1988, **27**, 7395.
6 K. S. Anderson and K. A. Johnson, *Chem. Rev.*, 1990, **90**, 1131.
7 K. A. Johnson, Z. B. Simpson and T. Blom, *Anal. Biochem.*, 2009, **387**, 20.
8 V. Klema and A. Laub, *IEEE Trans. Autom. Control*, 1980, **25**, 164–176.
9 E. R. Henry and J. Hofrichter, *Methods Enzymol.*, 1992, **210**, 129.
10 R. W. Hendler and R. I. Shrager, *J. Biochem. Biophys. Methods*, 1994, **28**, 1.
11 K. A. Johnson, Z. B. Simpson and T. Blom, *Anal. Biochem.*, 2009, **387**, 30.
12 L. De Lathauwer, B. De Moor and J. Vandewalle, *SIAM J. Matrix Anal. Appl.*, 2000, **21**, 1253.
13 G. H. Golub and C. Reinsch, *Numer. Math.*, 1970, **14**, 403.
14 I. M. Kolthoff and M. K. Chantooni, *J. Am. Chem. Soc.*, 1971, **93**, 3843.
15 O. Alter, P. O. Brown and D. Botstein, *Proc. Natl. Acad. Sci. U. S. A.*, 2000, **97**, 10101.
16 O. Troyanskaya, M. Cantor, G. Sherlock, P. Brown, T. Hastie, R. Tibshirani, D. Botstein and R. B. Altman, *Bioinformatics*, 2001, **17**, 520.
17 The KinTek Explorer kinetic modelling software fits kinetic and equilibrium data by nonlinear regression based on numerical integration of rate equations derived from a model input by the user.[7] For this study, the software was modified to enable the global fitting of time-resolved spectra collected at multiple concentrations of **DTT** to a single unifying model to define the pathway and rate constants of the **DTT**-induced declicking mechanism of **2Ph**-X.
18 E. Karnas, S. K. Kim, K. A. Johnson, J. L. Sessler, K. Ohkubo and S. Fukuzumi, *J. Am. Chem. Soc.*, 2010, **132**, 16617.